
Learning Multi-Agent Coordination through Graph-driven Communication

Emanuele Pesce
WMG
University of Warwick
Coventry, CV4 7AL
e.pesce@warwick.ac.uk

Giovanni Montana*
WMG
University of Warwick
Coventry, CV4 7AL
g.montana@warwick.ac.uk

Abstract

We discuss the problem of learning collaborative behaviour through communication in multi-agent systems using deep reinforcement learning. A connectivity-driven communication (CDC) algorithm is proposed to address three key aspects: what agents to involve in the communication, what information content to share, and how often to share it. The multi-agent system is modelled as a weighted graph with nodes representing agents. The unknown edge weights reflect the degree of communication between pairs of agents, which depends on a diffusion process on the graph - the heat kernel. An optimal communication strategy, tightly coupled with overall graph topology, is learned end-to-end concurrently with the agents' policy so as to maximise future expected returns. Empirical results show that CDC is capable of superior performance over alternative algorithms for a range of cooperative navigation tasks, and that the learned graph structures can be interpretable.

1 Introduction

In Deep Reinforcement Learning (RL), an agent learns to take sequential decisions by mapping its observations of the world to actions using a reward as feedback signal [46]. DRL has achieved unprecedented performance in many single-agent problems such as playing the game of Go [42], Atari videogames [34, 49], and autonomous robot locomotion [29]. Several real-world applications involve a team of multiple interacting agents that need to cooperatively accomplish a particular goal, e.g. in robot navigation [47], autonomous vehicles coordination [5], traffic management [12], supply chain management [28] and multi-player games [50].

Extensions of DRL to cooperative multi-agent domains have now started to emerge. One of the fundamental challenges in this context is how to provide the agents with the ability to develop adequate communication strategies. The fact that communication plays a critical role in achieving synchronization in multi-agent systems has been well documented [51, 11, 33, 21, 13, 45, 44, 38]. Three key aspects need to be considered: what messages need to be exchanged, when to share the messages, and with whom to communicate. The first problem - what to communicate - has been attacked in a number of different ways. For instance, by propagating the information through differential channels, the gradient is allowed to flow from agent to agent and provide appropriate feedback [13]. In [45], a neural network receives observations from all agents, and maps local messages onto a global message used to generate actions. Bidirectional recurrent neural networks have also been used to connect individual agent policies and Q-Networks, and implement communication mechanisms [37]. In [38], a memory device provides a shared communication channel used that each agents can use to extract informative content, and writes response messages.

The second issue - when to communicate - has been addressed through learnable attention units [20] or gating mechanisms deciding whether to allow or block messages [44]. Finally, the selection of agents involved in the communication has been implemented through attention

*Corresponding author

mechanisms that determine which interactions contribute the most to the overall performance [16] or to explicitly target agents for communication [9]. Related work in this direction has also suggested learnable scheduler units utilising a shared communication medium with limited bandwidth [22] and decentralized value functions that minimise inter-agent communication [52].

A number of graph-based approaches have appeared recently to address multi-agent DRL. For example, coordination graphs [14] have been used for sparse cooperative Q-learning [24] and to optimize the behaviour of traffic lights [27]. Graphs have been used to build multi-headed attention models [19], and attempts have been made to use graphs for modelling not only the agents, but also other entities in the environment [1].

In this paper, we propose a novel DRL framework for cooperative multi-agent scenarios that aims to improve coordination through a learned communication strategy, and addresses all three issues above - what, when and with whom to communicate. Our approach, Connectivity-driven Communication (CDC), makes use of a state-dependent weighted graph. Each node in the graph represents an agent, and an edge quantifies the degree of connectivity between pairs of agents. The edges of the graphs are learnt by the agents through continuous interactions with the environment, and give rise to varying network topologies. Our key observation is that a multi-agent system, as a whole, can be seen as a complex system represented as a graph. As such, an optimal communication mechanism should take into account the overall topological properties of the graph. Based on this observation, we model communication as a function of a diffusion process over the graph, which characterises the way in which the information flows. More specifically, we resort to the heat kernel of the graph to simulate a diffusion process of heat transference over time, which is then used by the agents to appropriately weight the messages received by adjacent nodes. Since communication is coupled with graph topology, learning how to communicate to solve a task implies that an optimal graph structure must be discovered for any given environmental state.

The proposed CDC algorithm is trained end-to-end, and builds on an extension of the actor-critic paradigm [10, 43, 29]. It is an instance of centralized-learning with decentralized-execution (CLDE) [13, 31] whereby additional information is used only during training, but not during execution. The performance of CDC has been evaluated against alternative methods on four cooperative navigation tasks. Our experimental evidence demonstrates that CDC is capable of outperforming other relevant state-of-the-art algorithms on different performance metrics. In addition, we analyse the communication patterns discovered by the agents to illustrate how interpretable topological structures can emerge in different scenarios.

2 Connectivity-driven Communication

2.1 Notation and problem setup

We consider Markov Games, a partially observable extension of Markov decision processes [30] involving N interacting agents. The environment states are contained in \mathcal{S} , and we use \mathcal{O}_i and \mathcal{A}_i to indicate the sets of all possible observations and actions for the i^{th} agent, with $i \in 1, \dots, N$, respectively. The agent-specific private representation of the state at time t is denoted as $\mathbf{o}_i^t \in \mathcal{O}_i$, and each action $a_i^t \in \mathcal{A}_i$ is deterministically determined by a mapping, $\mu_{\theta_i} : \mathcal{O}_i \mapsto \mathcal{A}_i$, parametrised by θ_i . A transition function $\mathcal{T} : \mathcal{S} \times \mathcal{A}_1 \times \mathcal{A}_2 \times \dots \times \mathcal{A}_N$ describes the stochastic behaviour of the environment. We model each agent as the node of an undirected weighted graph, $G^t = (V, \mathbf{S}^t)$, where V is the set of N nodes, and $\mathbf{S}^t \in [0, 1]^{V \times V}$ contains edge weights or connectivity strengths. In our formulation, each $\mathbf{S}^t(u, v) = \mathbf{S}^t(v, u) = s_{u,v}^t$ quantifies the degree of communication between a given pair of agents, u and v . We assume that each $s_{u,v}^t \in [0, 1]$ where values close to one indicate strong connectivity, and zero represents no connectivity. These weights are not known *a priori* and must be learnt. Our rationale is that, in order to decide how an agent's observation at a node should be shared with other agents, it is necessary to characterise how efficiently the information propagates

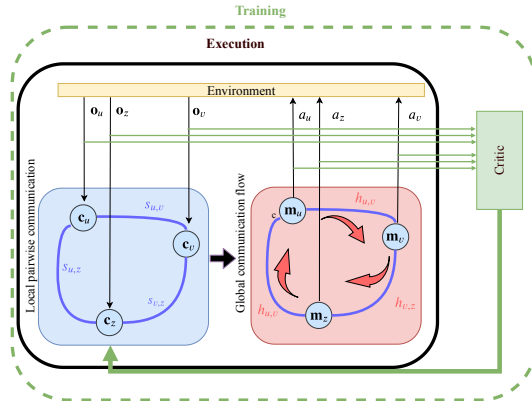


Figure 1: Diagrammatic representation of CDC.

throughout the entire graph. Since our communication mechanism relies directly on topological properties of the graph, learning the structure of the graph becomes central to efficient communication. This is elaborated further in Section 2.2.

Once the agent has received a message $\mathbf{m}_u^t \in \mathbb{R}^C$ containing the information from all the other agents, an action can be made as a deterministic function of the message, i.e.

$$a_u^t = \varphi_{\theta_u^p}(\mathbf{m}_u^t) \quad (1)$$

where $\varphi_{\theta_u^p}$ is a neural network with parameters θ_u^p . Once each agent has taken an action, a reward is provided by the environment, $r_i^t : \mathcal{S} \times \mathcal{A}_1 \times \mathcal{A}_2 \times \dots \times \mathcal{A}_N \mapsto \mathbb{R}$. Each agent objective's is to maximise the discounted sum of future rewards over time,

$$J(\theta_i) = \mathbb{E}_{a_1^t \sim \mu_1, \dots, a_N^t \sim \mu_N, s^t \sim \mathcal{T}} \left[\sum_{t=0}^T \gamma^t r_i^t(s^t, a_1^t, \dots, a_N^t) \right]$$

where $\gamma \in [0, 1]$ is the discount factor.

2.2 Learning the graph topology

We first explain how the weighted graph is generated at each time step. Given a pair of agents, u and v , their private observations are encoded to form a local message,

$$\mathbf{c}_{u,v}^t = \mathbf{c}_{v,u}^t = \varphi_{\theta^c}(\mathbf{o}_u^t, \mathbf{o}_v^t) \quad (2)$$

where φ_{θ^c} is a neural network with parameter θ^c . All the resulting messages are arranged in $\mathbf{C}^t \in \mathbb{R}^{V \times V \times C}$. Using this information, the connectivity weight between the corresponding nodes of the graph is given by

$$s_{u,v}^t = s_{v,u}^t = \sigma(\varphi_{\theta^s}(\mathbf{c}_{u,v}^t)) \quad (3)$$

where φ_{θ^s} is a neural network with parameter θ^s , and σ is a sigmoid function. The parameters required for learning the graph topology are in $\theta^g = \{\theta^s, \theta^c\}$.

2.3 Learning to communicate over graphs

Once the pair-wise connectivities in Eq. 3 have been determined, the graph is fully specified. A message-passing strategy is then introduced that takes into account the current network topology. Our observation here is that a diffusion process over the graph can help quantify how the information flows over G^t , and can inform a multi-agent communication strategy. Since the graph structure is being learnt by trial and error concurrently to the policy, our approach offers a mechanism to identify graph topologies that supports optimal communication for the task at hand. In this paper we make use of the heat kernel to simulate how the heat propagates throughout the network [25].

The heat flow of a graph is governed by its normalised Laplacian [41, 8]. The Laplacian of G^t is given by $\mathcal{L}^t = \mathbf{D}^t - \mathbf{S}^t$ where $\mathbf{D}^t(u, u) = \sum_{v \in V} s_{u,v}^t$ is the diagonal degree matrix of the graph. The normalised Laplacian is then obtained as $\hat{\mathcal{L}}^t = \frac{1}{\sqrt{\mathbf{D}^t}} \mathcal{L}^t \frac{1}{\sqrt{\mathbf{D}^t}}$ which is a fundamental term of the partial differential equation describing the heat diffusion process,

$$\frac{\partial H^t(p)}{\partial p} = -\hat{\mathcal{L}}^t H^t(p). \quad (4)$$

The heat kernel, $H^t(p) \in \mathbb{R}^{N \times N}$, is the fundamental solution representing the energy flowing through the network at time p . To avoid confusion, the environment time-step is denoted by t , and the time related to the diffusion process is denoted by p . The heat kernel is calculated by using the eigenspectrum formulation of the normalized Laplacian, $\hat{\mathcal{L}}^t = \phi^t \Lambda^t \phi^{t\top}$, in which $\Lambda^t = \text{diag}(\lambda_1^t, \dots, \lambda_N^t)$ is a diagonal matrix of eigenvalues ordered by increasing magnitude, and $\phi^t = (\phi_1^t, \dots, \phi_N^t)$ is a matrix with the corresponding eigenvector as columns. For each pair of nodes u and v , the respective heat kernel entry is given by

$$H^t(p)_{u,v} = \phi^t \exp[\Lambda^t p] \phi^{t\top} = \sum_{i=1}^{|V|} \exp[-\lambda_i^t p] \phi_i^t(u) \phi_i^t(v) \quad (5)$$

where $H(p)_{u,v}$ refers to the amount of heat that flowed from u and reached v at time p . This calculation can also be carried out using Padé approximant [2], given by $H(p) = \exp[-p \hat{\mathcal{L}}^t]$, which

is evaluated over a finite grid of P time points, and for every pair of u and v nodes. Additional details are provided in Section A of the Appendix.

For every pair of nodes, we select the time point p_s at which the heat transfer drops by a pre-determined percentage, s , and such that the flow becomes stable afterwards. This results in a matrix, \mathbf{H}^t , whose entries, $\mathbf{H}_{u,v}^t = H_{u,v}^t(p_s)$, are heat kernel values taken at such times, p_s , i.e.

$$p_s(u, v) = p_{max} : \left| \frac{H^t(p+1)_{u,v} - H^t(p)_{u,v}}{H^t(p)_{u,v}} \right| < s. \quad (6)$$

The heat kernel values are then used to determine a message-passing mechanism. Specifically, the aggregated information content for agent u is determined by a linear combination of pair-wise local messages from other agents,

$$\mathbf{m}_u^t = \sum_{v \in V} \mathbf{H}_{u,v}^t \mathbf{c}_{u,v}^t. \quad (7)$$

The message is then mapped on to actions though the non-linear mapping defined in Eq. 1. A lack of communication between a pair of agents results when no stable heat kernel values are found. Given two agents u, v , their respective entry in $\mathbf{H}_{u,v}^t$ will be zero if no value of $p_s(u, v)$ capable of satisfying Eq. 6 has been found. In this case the heat flow on the edge u, v would be not considered as stable and the communication along that link does not happen, leading to sparse patterns.

2.4 Reinforcement learning algorithm

In this section we describe how end-to-end learning is delivered. We extend the actor-critic framework [10], in which the actor produces actions and the critic returns feedback on the actor's moves. In our setting, multiple actors, one per every agent, receive feedback from a single centralised critic. In the standard DDPG [43, 29], the actor $\mu_\theta : \mathcal{O} \mapsto \mathcal{A}$ and the critic $Q^{\mu_\theta} : \mathcal{O} \times \mathcal{A} \mapsto \mathbb{R}$ functions are implemented through neural networks and aim to maximize the expected return $J(\theta) = \mathbb{E}[\sum_{i=1}^T r(\mathbf{o}^t, a^t)]$. The gradient $\nabla_\theta J(\theta)$ used to update θ is calculated as follows:

$$\nabla_\theta J(\theta) = \mathbb{E}_{\mathbf{o}^t \sim \mathcal{D}} [\nabla_\theta \mu_\theta(\mathbf{o}^t) \nabla_{a^t} Q^{\mu_\theta}(\mathbf{o}^t, a^t) |_{a^t = \mu_\theta(\mathbf{o}^t)}]$$

while Q^{μ_θ} is trained minimizing the following loss:

$$L(\theta) = \mathbb{E}_{\mathbf{o}^t, a^t, r^t, \mathbf{o}^{t+1} \sim \mathcal{D}} [(Q^{\mu_\theta}(\mathbf{o}^t, a^t) - y)^2]$$

where $y = r^t + \gamma Q^{\mu'_\theta}(\mathbf{o}^{t+1}, a^{t+1})$, $Q^{\mu'_\theta}$ is a target critic, whose parameters are only periodically updated with the parameters of Q^{μ_θ} , utilised to stabilize the training.

We follow the CLDE paradigm [26, 13, 31]. The critics are employed during learning, but otherwise only the actor and communication modules are used at test time. At training time, a centralised critic uses the observations and actions of all the agents to produce the Q value. In order to make the critic unique for all the agents and keep the number of parameters constant, we approximate our Q function using a recurrent neural network (RNN). We treat the observation/action pairs as a sequence with respect to the agents:

$$\mathbf{h}_i^t = \text{RNN}(\mathbf{o}_i^t, a_i^t | \mathbf{h}_{i-1}^t) \quad (8)$$

where \mathbf{h}_i^t and \mathbf{h}_{i-1}^t are the hidden state produced for the i^{th} and $i-1^{th}$ agent, respectively. Upon receiving all observation/action pairs from all agents, we use the last hidden state \mathbf{h}_N^t to produce the Q -value:

$$Q(\mathbf{o}_1^t, \dots, \mathbf{o}_N^t, a_1^t, \dots, a_N^t) = \varphi_{\theta_Q}(\mathbf{h}_N^t)$$

where φ is a neural network of parameters θ_Q . The parameters of the i^{th} agent are adjusted to maximize the objective function $J(\theta_i) = \mathbb{E}[R_i]$ following the direction of the gradient $J(\theta_i)$:

$$\nabla_{\theta_i} J(\theta_i) = \mathbb{E}_{\mathbf{o}_i^t, a_i^t, r^t, \mathbf{o}_i^{t+1} \sim \mathcal{D}} [\nabla_{\theta_i} \mu_{\theta_i}(\mathbf{m}_i^t) \nabla_{a_i^t} Q(\mathbf{x}) |_{a_i^t = \mu_{\theta_i}(\mathbf{m}_i^t)}]$$

where $\mathbf{x} = (\mathbf{o}_1^t, \dots, \mathbf{o}_N^t, a_1^t, \dots, a_N^t)$ and Q minimizes the temporal difference error as follows:

$$L(\theta_i) = \mathbb{E}_{\mathbf{o}_i^t, a_i^t, r^t, \mathbf{o}_i^{t+1} \sim \mathcal{D}} [(Q(\mathbf{x}) - y)^2]$$

in which:

$$y = r_i^t + \gamma Q(\mathbf{o}_1^{t+1}, \dots, \mathbf{o}_N^{t+1}, a_1^{t+1}, \dots, a_N^{t+1})$$

The pseudo-code summarising the proposed learning algorithm is provided in Section B of the Appendix. The proposed architecture is summarised in Figure 1.

3 Experimental results

3.1 Environments

The performance of CDC has been assessed in four different environments. Three of them are commonly used swarm robotic benchmarks - *Navigation Control*, *Formation Control* and *Line Control* [32, 3, 1]. A fourth one, *Pack Control*, has been added to provide a more challenging task. All the environments have been tested using the Multi-Agent Particle Environment [31, 35], which allows agents to move around in two-dimensional spaces with discretised action spaces. In *Navigation Control* the agents must move closer to all landmarks whilst avoiding collisions; in *Formation Control* and *Line Control* they must navigate in order to form a polygonal geometric shape centred around the landmark and position themselves along the straight line connecting the two landmarks, respectively; in *Dynamic Pack Control*, worker agents need to follow the leaders to occupy a landmark, that once taken, moves to a different location. Further details are given in the Appendix, Section G.

For each environment we have tested two versions with different number of agents: a *basic* one focusing on solving the designed task when only 3 – 4 agents are involved, and a *scalable* one to show the ability to succeed with a higher number (8 – 10) of agents. The performance of competing MARL algorithms has been assessed using a number of metrics: the *reward*, which quantifies how well a task has been solved (the higher the better); the *distance*, which indicates the amount of navigation carried out by the agents to solve the task (the lower the better); the number of *collisions*, which shows the ability to avoid collisions (the lower the better); the *time* required to solve the task (the lower the better); the *success rate*, defined as the number of times an algorithm has solved a task over the total number of attempts; and *caught targets*, which refers to the number of landmarks that the pack managed to reach. Illustrative videos showing CDC in action on the above environments can be found online².

3.2 Experimental Setup

For our experiments, we use neural networks with two hidden layers (64 each) to implement the graph generation modules (Eq. 3, 2) and the action selector in Eq. 1. The RNN described in Equation 8 is implemented as a long-short term memory (LSTM) network [39] with 64 units for the hidden state.

We use the Adam optimizer [23] with a learning rate of 10^{-3} for critic and 10^{-4} for policies. Similarly to [1, 53], we set $\theta_1 = \theta_2 = \dots = \theta_N$ in order to make the model invariant to the number of agents. The reward discount factor is set to 0.95, the size of the replay buffer to 10^6 , and the batch size to 1,024. At each iteration, we calculate the heat kernel over a finite grid of $P = 300$ time points, with a threshold for getting stable values set to $s = 0.05$. This value has been determined experimentally (see Section E of the Appendix). The number of time steps for episode, T , is set to 50 for all the environments, except for Navigation Control where is set to 25. For Formation Control, Line Control and Pack Control the number E of episodes is set to 50,000 for the basic versions (30,000 for scalable versions), while for Navigation Control is set to 100,000 (30,000 for scalable versions). All network parameters are updated every time 100 new samples are added to the replay buffer. Soft updates with target networks use $\tau = 0.01$. We adopt the low-variance gradient estimator Gumbel-Softmax for discrete actions in order to allow the back-propagation to work properly with categorical variable, which can truncate the gradient's flow. All the presented results are produced by running every experiment 5 times with different seeds (1,2001,4001,6001,8001) in order to avoid that a particular choice of the seed can significantly condition the final performance. Python 3.6.6 [48] with PyTorch 0.4.1 [36] is used as framework for machine learning and automatic differentiable computing. NetworkX 2.2 [15] has been used for graph analysis. Computations were mainly performed using Intel(R) Xeon(R) CPU E5-2650 v3 at 2.30GHz as CPU and GeForce GTX TITAN X as GPU. With this configuration, the proposed CDC in average took approximately 8.3 hours to complete a training procedure on environments with four agents involved.

3.3 Main results

We have compared CDC against five different baselines, each one representing a different way to approach the MA coordination problem: independent DDPG [43, 29], MADDPG [31], CommNet

²<http://bit.ly/37d5Jum>

	Navigation Control $N = 3$			Navigation Control $N = 10$		
	Reward	# collisions	Distance	Reward	# collisions	Distance
DDPG	-57.3 ± 9.94	1.24 ± 0.39	4.09 ± 6.92	-115.93 ± 21.26	8.83 ± 6.41	3.6 ± 0.85
MADDPG	-45.23 ± 6.59	0.77 ± 0.24	3.16 ± 5.74	-112.17 ± 13.23	12.29 ± 7.45	3.44 ± 0.53
CommNet	-48.95 ± 6.25	0.92 ± 0.24	3.49 ± 5.09	-104.49 ± 10.45	12.21 ± 6.87	3.14 ± 0.41
MAAC	-43.18 ± 6.44	0.71 ± 0.24	1.46 ± 2.97	-107.38 ± 11.81	9.04 ± 6.46	3.26 ± 0.46
ST-MARL	-55.36 ± 8.17	1.54 ± 3.56	1.2 ± 0.33	-110.69 ± 15.75	32.73 ± 32.77	3.27 ± 0.57
CDC	-39.16 ± 4.77	0.56 ± 0.19	0.4 ± 1.66	-102.68 ± 10.1	9.03 ± 9.36	3.06 ± 0.4
	Formation Control $N = 4$			Formation Control $N = 10$		
	Reward	Time	Success Rate	Reward	Time	Success Rate
DDPG	-39.43 ± 12.37	50 ± 0.0	0 ± 0.0	-49.27 ± 6.11	50 ± 0.0	0 ± 0.0
MADDPG	-19.86 ± 6.04	50 ± 0.0	0 ± 0.0	-20.65 ± 7.11	50 ± 0.0	0 ± 0.0
CommNet	-7.77 ± 2.06	45.8 ± 10.19	0.180.38	-10.22 ± 1.03	48.89 ± 5.5	0.04 ± 0.2
MAAC	-5.77 ± 1.53	26.66 ± 17.2	0.66 ± 0.47	-9.63 ± 1.35	50 ± 0.0	0 ± 0.0
ST-MARL	-20.24 ± 3.0	50 ± 0.0	0 ± 0.0	-19.81 ± 5.74	50 ± 0.0	0 ± 0.0
CDC	-4.22 ± 1.46	11.82 ± 5.49	0.99 ± 0.12	-7.51 ± 1.06	15.21 ± 9.23	0.99 ± 0.1
	Line Control $N = 4$			Line Control $N = 10$		
	Reward	Time	Success Rate	Reward	Time	Success Rate
DDPG	-33.45 ± 10.58	49.99 ± 0.22	0 ± 0.0	-68.19 ± 10.2	50 ± 0.0	0 ± 0.0
MADDPG	11.55 ± 2.79	47.32 ± 9.14	0.08 ± 0.27	-12.69 ± 2.11	48.48 ± 7.12	0.04 ± 0.21
CommNet	-10.99 ± 2.24	46.97 ± 8.93	0.12 ± 0.33	-9.58 ± 1.28	37.73 ± 14.85	0.47 ± 0.5
MAAC	-7.38 ± 2.09	17.08 ± 12.17	0.89 ± 0.32	-8.58 ± 1.52	22.55 ± 16.09	0.76 ± 0.43
ST-MARL	-23.87 ± 7.77	50 ± 0.0	0 ± 0.0	-19.24 ± 6.26	50 ± 0.0	0 ± 0.0
CDC	-5.97 ± 1.73	10.42 ± 5.58	0.98 ± 0.13	-7.96 ± 1.19	15.06 ± 12.02	0.91 ± 0.29
	Dynamic Pack Control $N = 4$			Dynamic Pack Control $N = 8$		
	Reward	Distance	Targets caught	Reward	Distance	Targets caught
DDPG	-224.77 ± 87.65	3.52 ± 1.67	0 ± 0.0	-279.67 ± 70.18	4.58 ± 1.4	0 ± 0.0
MADDPG	-116.15 ± 71.37	1.46 ± 0.72	0.2 ± 0.13	-110.86 ± 28.66	1.22 ± 0.28	0.0 ± 0.05
CommNet	293.35 ± 446.89	1.11 ± 0.12	0.81 ± 0.89	-76.18 ± 138.73	1.13 ± 0.25	0.07 ± 0.28
MAAC	-95.29 ± 61.65	1.25 ± 0.21	0.01 ± 0.12	-105.15 ± 46.42	1.15 ± 0.28	0.01 ± 0.09
ST-MARL	-107.02 ± 71.84	1.26 ± 0.3	0.02 ± 0.14	-123.91 ± 16.89	1.42 ± 0.36	0 ± 0.0
CDC	369.5 ± 463.92	1.09 ± 0.1	0.96 ± 0.93	58.03 ± 279.05	1.12 ± 0.14	0.35 ± 0.56

Table 1: Comparison of DDPG, MADDPG, CommNet, MAAC, ST-MARL and CDC on all four environments and using two different number of agents in each case. Results are averaged over five different seeds.

[45], MAAC [17] and ST-MARL [53]. Independent DDPG provides the simplest baseline in that each agent works independently to solve the task. In MADDPG each agent has its own critic with access to combined observations and actions from all agents during learning. CommNet implements an explicit form of communication. The policies are implemented through a large neural network with some components of the networks shared across all the agents and others agent-specific. At every time-step each agent’s action depends on the local observation, and on the average of all other policies (neural network hidden states), used as messages. MAAC is a state-of-the art method in which an attention mechanism guides the critics to select the information to be shared with the actors. ST-MARL uses a graph neural network to capture the spatio-temporal dependency of the observations and facilitate cooperation. Unlike our approach, the graph edges here represents the time-depending agents’ relationships, and capture the spatial and temporal dependencies amongst agents. Table 1 summarises the experimental results obtained from all algorithms across all the environments. The metric values are obtained by executing the best model (chosen according to the best average reward returned during training) for an additional 100 episodes. We repeated each experiment using 5 different seeds, and each entry of Table 1 is an average over 500 values. It can be noted that CDC outperforms the five competitors on all four environments on all the metrics. In Navigation Control ($N = 3$), the task is solved by minimizing the overall distance travelled and the number of collisions, with an improvement over MAAC. In Formation Control ($N = 4$), the best performance is also achieved by CDC, which always succeeded in half of time compared to MAAC. On this task, CommNet performs poorly, and DDPG and MADDPG completely fail.

When the number of agents is increased, and the level of difficulty is significantly higher, all the baselines fail to complete the task whilst CDC still maintains excellent performance with a success rate of 0.99. In Line Control, both scenarios ($N = 4$ and $N = 10$) are efficiently solved by CDC with higher success rate and less time compared to MAAC, while all other algorithms fail. For Dynamic Pack Control, amongst the competitors, only CommNet does not fail. In this environment, only the leaders can see the point of interest, hence the other agents must learn how to communicate with them. In this case, CDC also outperforms CommNet on both the number of targets that are being caught and travelled distance. Overall, it can be noted that the gains in performance achieved by CDC, compared to other methods, significantly increase when increasing the number of agents.

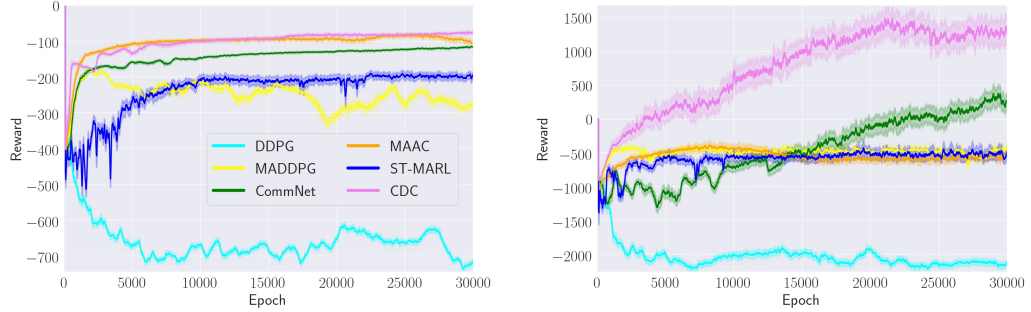


Figure 2: Learning curves for comparison algorithms on Formation Control and Dynamic Pack Control. On the x-axis the number of episodes and on y-axis the achieved rewards. Results are averaged over five different runs.

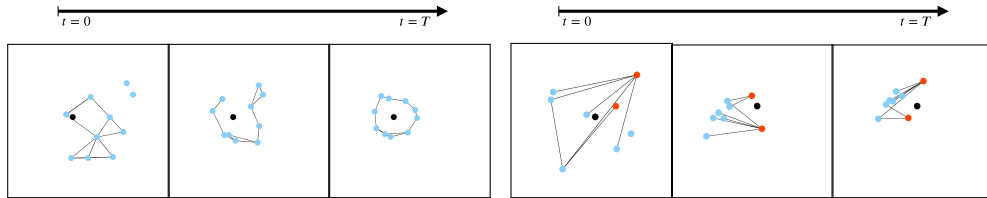


Figure 3: Illustrations of communication networks G_H^t evolving over different episode time-steps on Formation Control and Dynamic Pack Control.

Learning curves for Formation Control and Dynamic Pack Control, averaged over five runs, are shown in Figure 2 (see also the Appendix, Section C.1, for other environments). Here it can be noticed that CDC reaches the highest reward overall. The Dynamic Pack Control task is particularly interesting as only two methods are capable of solving it, CommNet and CDC, and both of them implement explicit communication mechanisms. With only 4 agents, the reward curves of CommNet, MAAC, and CDC tend to be approximately similar, but increasing the numbers of agents to 8 highlights the remarkable benefits introduced by CDC. The high variance associated with CDC and CommNet in Dynamic Pack Control can be explained by the fact that, when a landmark is reached by all the agents, the environment returns a higher reward. These are the only two methods capable of solving the task, and lower variance is associated to other methods that perform poorly. The performance of CDC when varying the number of agents at execution time is investigated (see Appendix, Section F).

3.4 Communication analysis

In this section, we provide an initial qualitative evaluation of the communication patterns and associated topological structures that have emerged using CDC on the four environments. Figure 3 shows the communication networks G_H^t evolving over time at a given episode during execution: black circles represent the landmarks, blue circles indicate the normal agents, and the red circles are the leaders. Their coordinates within the two-dimensional area indicate the navigation trajectories. The lines connecting pairs of agents represent the time-varying edge weights, H^t . Each $H_{u,v}^t$ element quantifies the amount of diffused heat between the two nodes, and Figure 3 illustrates how those quantities evolve over time. This figure can help interpret which agents are involved in the communication at any given time.

As expected, different patterns emerge in different environments. Figure 3(a) shows that, in Formation Control, the dynamic graphs are highly connected in the early stages of the episodes, and are sparser later on when the formation is found. The degree of topological adjustment observed over time indicate initial bursts of communication activity at the beginning of an episode, while towards the end the communication mostly consists of messages shared across neighbours, which seems to be sufficient to maintain the polygonal shape. A different situation can be observed in Dynamic Pack Control, in Figure 3(b). In this case, an intense communication activity emerges between leaders and members from an early stage, and the emerging topology approximates a bipartite graph between red and blue nodes. This is an expected and plausible pattern, given the nature of this environment. Solving this task

requires that the leaders share information with the members, which otherwise would not know the landmark location. Patterns observed in other environments are reported in the Appendix, Section C.2.

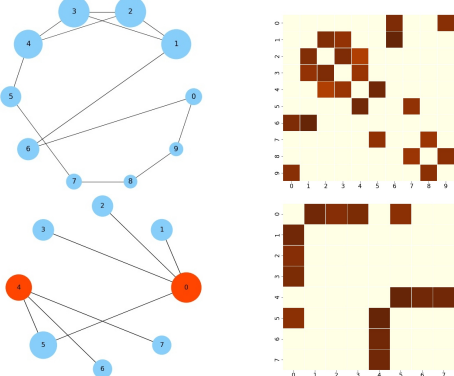


Figure 4: Averaged communication graphs for Formation Control (line above) and Pack Control (line below).

Further appreciation for the role played by the heat kernel in driving the communication strategy can be gained by observing Figure 4 which provides visualisations for two environments (other environments are reported in Section C.3 of the Appendix). On the left, the connection weights are visualised using a circular layout. Here the nodes represent agents, and the size of each node is proportional to the node’s eigenvector centrality. The eigenvector centrality is a popular graph spectral measure [4], utilised to determine the influence of a node considering both its adjacent connections and the importance of its neighbouring node. This measure is calculated using the stable heat diffused values averaged over an episode, i.e. $\mathbf{H}_{u,v} = (\sum_{t=1}^T \mathbf{H}_{u,v}^t)/T$. The resulting graph structure reflects the overall communication patterns emerged while solving

the given tasks. On the right, we visualise the squared $N \times N$ matrix of averaged pairwise diffusion values as a heatmap (red values are higher). It can be noted that, in Pack Control, two communities of agents are formed, each one with a leader. Here, as expected, leaders appear to be very influential nodes (red nodes), and the heatmap shows that the connections between individual members and leaders are very strong. A different pattern emerges instead in Formation Control, where there is no evidence of communities since all nodes are connected to nearly form a circular shape. The corresponding heatmap shows the heat kernel values connecting neighbouring agents tend to assume higher values compared to more distant agents.

4 Conclusions

In this work, we have presented a novel approach to deep multi-agent reinforcement learning that models agents as nodes of a graph, and uses the overall topology of the graph to facilitate communication and cooperation. As far as we are aware, this is the first attempt to explicitly couple inter-agent communication with overall graph topology using a diffusion process over the graph, and to use an end-to-end learning algorithm to optimise the agents’ policies concurrently with the graph structures. The resulting CDC algorithm equips the agents with a mechanism to learn what messages should be shared with others, how often, and with whom, using the learnt heat kernel to weight every agent’s contribution during communication.

Our experimental results on four different environments have demonstrated that, compared to other baselines, CDC can achieve superior performance on navigation tasks of increasing complexity, and remarkably so when the number of agents increases. We have also found that visualising the graphs learnt by the agents can shed some light on the role played by the diffusion process in mediating the communication strategy that ultimately yields highly rewarding policies. This work represents an initial attempt to leverage graph-theoretic properties in the context of a multi-agent communication strategy, and paves the way for future exploration along related directions. For instance, further constraints could be imposed on the graph edges to regulate the overall communication process, e.g. using a notion of flow conservation [18].

5 Ethical Statement

In terms of societal consequences, the broader impact of CDC strictly depends on the nature of the application for which it is used. Improving the effectiveness of agents’ navigation would mostly be beneficial for our society when this type of technology is aimed at easing the job done by humans or delivering better services. For example, the Line Control environment we have discussed could represent two workers who learn how to replace broken bridges in case of an emergency. A possible negative use of this technology may be related to activities aiming to invade privacy, for example optimizing the exchange and diffusion of illegally gathered information. As with any technology, its wider societal consequences strictly depend on one’s intention when adopting them.

References

- [1] Akshat Agarwal, Sumit Kumar, and Katia Sycara. Learning transferable cooperative behavior in multi-agent teams. *arXiv preprint arXiv:1906.01202*, 2019.
- [2] Awad H Al-Mohy and Nicholas J Higham. A new scaling and squaring algorithm for the matrix exponential. *SIAM Journal on Matrix Analysis and Applications*, 31(3):970–989, 2009.
- [3] Tucker Balch and Ronald C Arkin. Behavior-based formation control for multirobot teams. *IEEE transactions on robotics and automation*, 14(6):926–939, 1998.
- [4] Phillip Bonacich. Some unique properties of eigenvector centrality. *Social networks*, 29(4):555–564, 2007.
- [5] C-A Brunet, Ruben Gonzalez-Rubio, and Mario Tetreault. A multi-agent architecture for a driver model for autonomous road vehicles. In *Proceedings 1995 Canadian Conference on Electrical and Computer Engineering*, volume 2, pages 772–775. IEEE, 1995.
- [6] Alexander H-D Cheng and Daisy T Cheng. Heritage and early history of the boundary element method. *Engineering Analysis with Boundary Elements*, 29(3):268–302, 2005.
- [7] Ai Wern Chung, MD Schirmer, Michelle L Krishnan, Gareth Ball, Paul Aljabar, A David Edwards, and Giovanni Montana. Characterising brain network topologies: a dynamic analysis approach using heat kernels. *Neuroimage*, 141:490–501, 2016.
- [8] Fan RK Chung and Fan Chung Graham. *Spectral graph theory*. Number 92. American Mathematical Soc., 1997.
- [9] Abhishek Das, Théophile Gervet, Joshua Romoff, Dhruv Batra, Devi Parikh, Michael Rabat, and Joelle Pineau. Tarmac: Targeted multi-agent communication. *arXiv preprint arXiv:1810.11187*, 2018.
- [10] Thomas Degris, Martha White, and Richard S Sutton. Off-policy actor-critic. *arXiv preprint arXiv:1205.4839*, 2012.
- [11] Stefano Demichelis and Jorgen W Weibull. Language, meaning, and games: A model of communication, coordination, and evolution. *American Economic Review*, 98(4):1292–1311, 2008.
- [12] Kurt Dresner and Peter Stone. Multiagent traffic management: A reservation-based intersection control mechanism. In *Proceedings of the Third International Joint Conference on Autonomous Agents and Multiagent Systems-Volume 2*, pages 530–537. IEEE Computer Society, 2004.
- [13] Jakob Foerster, Ioannis Alexandros Assael, Nando de Freitas, and Shimon Whiteson. Learning to communicate with deep multi-agent reinforcement learning. In *Advances in Neural Information Processing Systems*, pages 2137–2145, 2016.
- [14] Carlos Guestrin, Daphne Koller, and Ronald Parr. Multiagent planning with factored mdps. In *Advances in neural information processing systems*, pages 1523–1530, 2002.
- [15] Aric Hagberg, Pieter Swart, and Daniel S Chult. Exploring network structure, dynamics, and function using networkx. Technical report, Los Alamos National Lab.(LANL), Los Alamos, NM (United States), 2008.
- [16] Yedid Hoshen. Vain: Attentional multi-agent predictive modeling. In *Advances in Neural Information Processing Systems*, pages 2701–2711, 2017.
- [17] Shariq Iqbal and Fei Sha. Actor-attention-critic for multi-agent reinforcement learning. *ICML*, 2019.
- [18] Junteng Jia, Michael T Schaub, Santiago Segarra, and Austin R Benson. Graph-based semi-supervised & active learning for edge flows. In *Proceedings of the 25th ACM SIGKDD International Conference on Knowledge Discovery & Data Mining*, pages 761–771, 2019.

- [19] Jiechuan Jiang, Chen Dun, and Zongqing Lu. Graph convolutional reinforcement learning for multi-agent cooperation. *arXiv preprint arXiv:1810.09202*, 2(3), 2018.
- [20] Jiechuan Jiang and Zongqing Lu. Learning attentional communication for multi-agent cooperation. *arXiv preprint arXiv:1805.07733*, 2018.
- [21] Michael Kearns. Experiments in social computation. *Communications of the ACM*, 55(10):56–67, 2012.
- [22] Daewoo Kim, Sangwoo Moon, David Hostallero, Wan Ju Kang, Taeyoung Lee, Kyunghwan Son, and Yung Yi. Learning to schedule communication in multi-agent reinforcement learning. *arXiv preprint arXiv:1902.01554*, 2019.
- [23] Diederik P Kingma and Jimmy Ba. Adam: A method for stochastic optimization. *arXiv preprint arXiv:1412.6980*, 2014.
- [24] Jelle R Kok and Nikos Vlassis. Collaborative multiagent reinforcement learning by payoff propagation. *Journal of Machine Learning Research*, 7(Sep):1789–1828, 2006.
- [25] R Kondor and J Lafferty. Diffusion kernels on graphs and other discrete input spaces. *icml 2002. In Proc*, pages 315–322, 2002.
- [26] Landon Kraemer and Bikramjit Banerjee. Multi-agent reinforcement learning as a rehearsal for decentralized planning. *Neurocomputing*, 190:82–94, 2016.
- [27] Lior Kuyer, Shimon Whiteson, Bram Bakker, and Nikos Vlassis. Multiagent reinforcement learning for urban traffic control using coordination graphs. In *Joint European Conference on Machine Learning and Knowledge Discovery in Databases*, pages 656–671. Springer, 2008.
- [28] J-H Lee and C-O Kim. Multi-agent systems applications in manufacturing systems and supply chain management: a review paper. *International Journal of Production Research*, 46(1):233–265, 2008.
- [29] Timothy P. Lillicrap, Jonathan J. Hunt, Alexander Pritzel, Nicolas Heess, Tom Erez, Yuval Tassa, David Silver, and Daan Wierstra. Continuous control with deep reinforcement learning. *CoRR*, abs/1509.02971, 2015.
- [30] Michael L Littman. Markov games as a framework for multi-agent reinforcement learning. In *Machine Learning Proceedings 1994*, pages 157–163. Elsevier, 1994.
- [31] Ryan Lowe, Yi Wu, Aviv Tamar, Jean Harb, OpenAI Pieter Abbeel, and Igor Mordatch. Multi-agent actor-critic for mixed cooperative-competitive environments. In *Advances in Neural Information Processing Systems*, pages 6379–6390, 2017.
- [32] Mehran Mesbahi and Magnus Egerstedt. *Graph theoretic methods in multiagent networks*, volume 33. Princeton University Press, 2010.
- [33] John H Miller and Scott Moser. Communication and coordination. *Complexity*, 9(5):31–40, 2004.
- [34] Volodymyr Mnih, Koray Kavukcuoglu, David Silver, Andrei A Rusu, Joel Veness, Marc G Bellemare, Alex Graves, Martin Riedmiller, Andreas K Fidjeland, Georg Ostrovski, et al. Human-level control through deep reinforcement learning. *Nature*, 518(7540):529, 2015.
- [35] Igor Mordatch and Pieter Abbeel. Emergence of grounded compositional language in multi-agent populations. *arXiv preprint arXiv:1703.04908*, 2017.
- [36] Adam Paszke, Sam Gross, Soumith Chintala, Gregory Chanan, Edward Yang, Zachary DeVito, Zeming Lin, Alban Desmaison, Luca Antiga, and Adam Lerer. Automatic differentiation in pytorch, 2017.
- [37] Peng Peng, Quan Yuan, Ying Wen, Yaodong Yang, Zhenkun Tang, Haitao Long, and Jun Wang. Multiagent bidirectionally-coordinated nets for learning to play starcraft combat games. *arXiv preprint arXiv:1703.10069*, 2017.

[38] Emanuele Pesce and Giovanni Montana. Improving coordination in multi-agent deep reinforcement learning through memory-driven communication. *Deep Reinforcement Learning Workshop, (NeurIPS 2018), Montreal, Canada*, 2019.

[39] Jurgen Schmidhuber. A general method for multi-agent reinforcement learning in unrestricted environments. In *Adaptation, Coevolution and Learning in Multiagent Systems: Papers from the 1996 AAAI Spring Symposium*, pages 84–87, 1996.

[40] Richard Schoen and Chris A Shing-Tung Yau Mack. *Lectures on Differential Geometry*. International Press, 1994.

[41] Richard Schoen and Shing-Tung Yau. *Lectures on differential geometry*, volume 2. International press Cambridge, MA, 1994.

[42] David Silver, Aja Huang, Chris J Maddison, Arthur Guez, Laurent Sifre, George Van Den Driessche, Julian Schrittwieser, Ioannis Antonoglou, Veda Panneershelvam, Marc Lanctot, et al. Mastering the game of go with deep neural networks and tree search. *nature*, 529(7587):484, 2016.

[43] David Silver, Guy Lever, Nicolas Heess, Thomas Degris, Daan Wierstra, and Martin Riedmiller. Deterministic policy gradient algorithms. In *ICML*, 2014.

[44] Amanpreet Singh, Tushar Jain, and Sainbayar Sukhbaatar. Learning when to communicate at scale in multiagent cooperative and competitive tasks. *ICLR*, 2019.

[45] Sainbayar Sukhbaatar, Rob Fergus, et al. Learning multiagent communication with backpropagation. In *Advances in Neural Information Processing Systems*, pages 2244–2252, 2016.

[46] Richard S Sutton and Andrew G Barto. *Introduction to reinforcement learning*, volume 135. MIT press Cambridge, 1998.

[47] Herbert G Tanner and Amit Kumar. Towards decentralization of multi-robot navigation functions. In *Proceedings of the 2005 IEEE International Conference on Robotics and Automation*, pages 4132–4137. IEEE, 2005.

[48] Guido Van Rossum and Fred L Drake Jr. *Python tutorial*. Centrum voor Wiskunde en Informatica Amsterdam, The Netherlands, 1995.

[49] Oriol Vinyals, Igor Babuschkin, Wojciech M Czarnecki, Michaël Mathieu, Andrew Dudzik, Junyoung Chung, David H Choi, Richard Powell, Timo Ewalds, Petko Georgiev, et al. Grandmaster level in starcraft ii using multi-agent reinforcement learning. *Nature*, pages 1–5, 2019.

[50] Oriol Vinyals, Timo Ewalds, Sergey Bartunov, Petko Georgiev, Alexander Sasha Vezhnevets, Michelle Yeo, Alireza Makhzani, Heinrich Küttler, John Agapiou, Julian Schrittwieser, et al. Starcraft ii: A new challenge for reinforcement learning. *arXiv preprint arXiv:1708.04782*, 2017.

[51] Yevgeniy Vorobeychik, Zlatko Joveski, and Sixie Yu. Does communication help people coordinate? *PloS one*, 12(2):e0170780, 2017.

[52] Tonghan Wang, Jianhao Wang, Chongyi Zheng, and Chongjie Zhang. Learning nearly decomposable value functions via communication minimization. *arXiv preprint arXiv:1910.05366*, 2019.

[53] Yanan Wang, Tong Xu, Xin Niu, Chang Tan, Enhong Chen, and Hui Xiong. Stmarl: A spatio-temporal multi-agent reinforcement learning approach for traffic light control. *arXiv preprint arXiv:1908.10577*, 2019.

[54] Bai Xiao, Richard C Wilson, and Edwin R Hancock. Characterising graphs using the heat kernel. 2005.

Appendix

A Heat kernel: additional details

The heat kernel is a technique from spectral geometry [40], and is a fundamental solution of the *heat equation*:

$$\frac{\partial H^t(p)}{\partial p} = -\hat{\mathcal{L}}^t H^t(p). \quad (9)$$

Given a graph G defined on n vertices, the normalized Laplacian $\hat{\mathcal{L}}$, acting on functions with Neumann boundary conditions [6], is associated with the rate of heat dissipation. $\hat{\mathcal{L}}$ can be written as:

$$\hat{\mathcal{L}} = \sum_{i=0}^{n-1} \lambda_i I_i$$

where I_i is the projection onto the i^{th} eigenfunction ϕ_i . For a given time $t \geq 0$, the heat kernel $H(t)$ is defined as a $n \times n$ matrix:

$$H(t) = \sum_i \exp[-\lambda_i t] I_i = \exp[-t\hat{\mathcal{L}}]. \quad (10)$$

Eq. 10 represents an analytical solution to Eq. 9.

Lemma 1 [8] *The heat kernel $H(t)$ for a graph G with eigenfunctions θ_i satisfies:*

$$H(t)_{u,v} = \sum_{i=1} \exp[-\lambda_i t] \phi_i(u) \phi_i(v)$$

The proof follows from the fact that

$$H(t) = \sum_i \exp[-\lambda_i t] I_i$$

and

$$I(u, v) = \phi_i(u) \phi_i(v).$$

Lemma 1 is provided to explain Eq. 5.

B Pseudo-code

Algorithm 1 CDC

```

1: Inizialise actor ( $\mu_{\theta_1}, \dots, \mu_{\theta_N}$ ) and critic networks ( $Q_{\theta_1}, \dots, Q_{\theta_N}$ )
2: Inizialise actor target networks ( $\mu'_{\theta_1}, \dots, \mu'_{\theta_N}$ ) and critic target networks ( $Q'_{\theta_1}, \dots, Q'_{\theta_N}$ )
3: Inizialise replay buffer  $\mathcal{D}$ 
4: for episode = 1 to E do
5:   Reset environment,  $\mathbf{o}^1 = \mathbf{o}_1^1, \dots, \mathbf{o}_N^1$ 
6:   for t = 1 to T do
7:     Generate  $\mathbf{C}^t$  (Eq. 2) and  $\mathbf{S}^t$  (Eq. 3)
8:     for p = 1 to P do
9:       Compute Heat Kernel  $H(p)^t$  (Eq. 4)
10:    end for
11:    Build  $\mathbf{H}^t$  with stable Heat Kernel values (Eq. 6)
12:    for agent i = 1 to N do
13:      Produce agent's message  $\mathbf{m}_i^t$  (Eq. 7)
14:      Select action  $a_i^t = \mu_{\theta_i}(\mathbf{m}_i^t)$ 
15:    end for
16:    Execute  $\mathbf{a}^t = (a_1^t, \dots, a_N^t)$ , observe r and  $\mathbf{o}^{t+1}$ 
17:    Store transaction  $(\mathbf{o}^t, \mathbf{a}^t, r, \mathbf{o}^{t+1})$  in  $\mathcal{D}$ 
18:  end for
19:  for agent i = 1 to N do
20:    Sample minibatch  $\Theta$  of B transactions  $(\mathbf{o}, \mathbf{a}, r, \mathbf{o}')$ 
21:    Update critic by minimizing:
22:
23:     $L(\theta_i) = \frac{1}{B} \sum_{(\mathbf{o}, \mathbf{a}, r, \mathbf{o}') \in \Theta} (y - Q(\mathbf{o}, \mathbf{a}))^2$ ,
24:    where  $y = r_i + \gamma Q(\mathbf{o}', \mathbf{a}')|_{a_k' = \mu'_{\theta_k}(\mathbf{m}'_k)}$ 
25:    in which  $\mathbf{m}'_k$  is global message computed using target networks
26:    Update actor according to the policy gradient:
27:     $\nabla_{\theta_i} J \approx \frac{1}{B} \sum \left( \nabla_{\theta_i} \mu_{\theta_i}(\mathbf{m}_i) \nabla_{a_i} Q^{\mu_{\theta_i}}(\mathbf{o}, \mathbf{a})|_{a_i = \mu_{\theta_i}(\mathbf{m}_i)} \right)$ 
28:  end for
29:  Update target networks:
30:   $\theta_i' = \tau \theta_i + (1 - \tau) \theta_i'$ 
31: end for

```

C Additional results

C.1 Learning curves

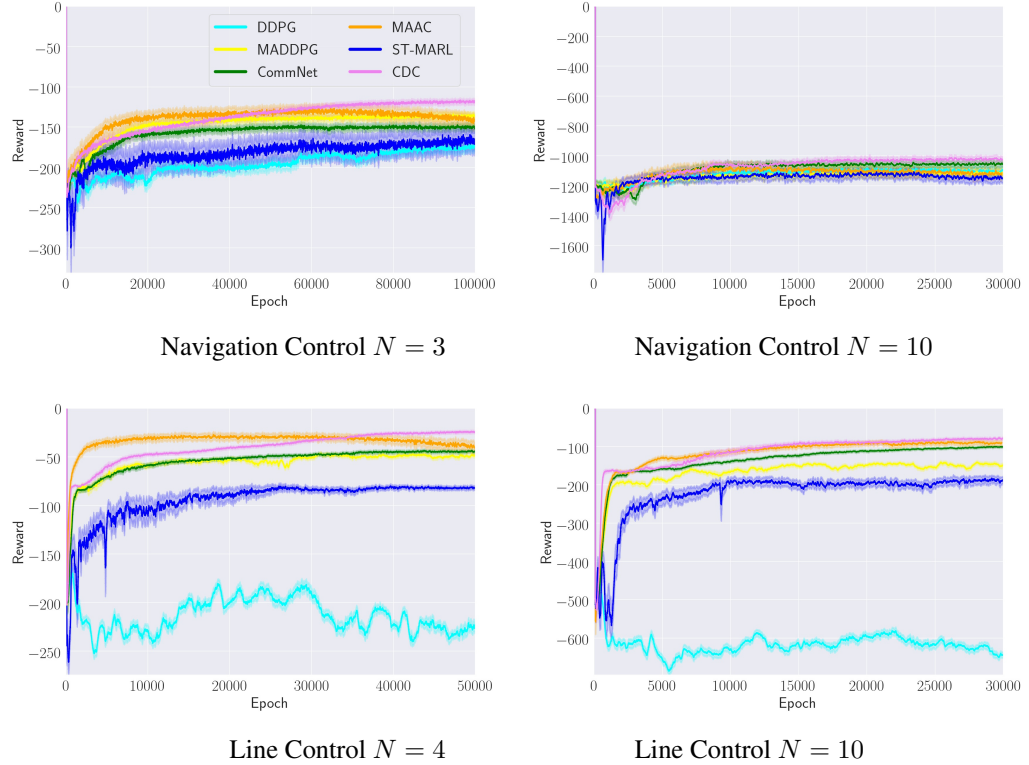


Figure 5: Learning curves for 6 competing algorithms assessed on Navigation Control and Line Control. Horizontal axes report the number of episodes, while vertical axes the achieved rewards. Results are averaged over five different runs.

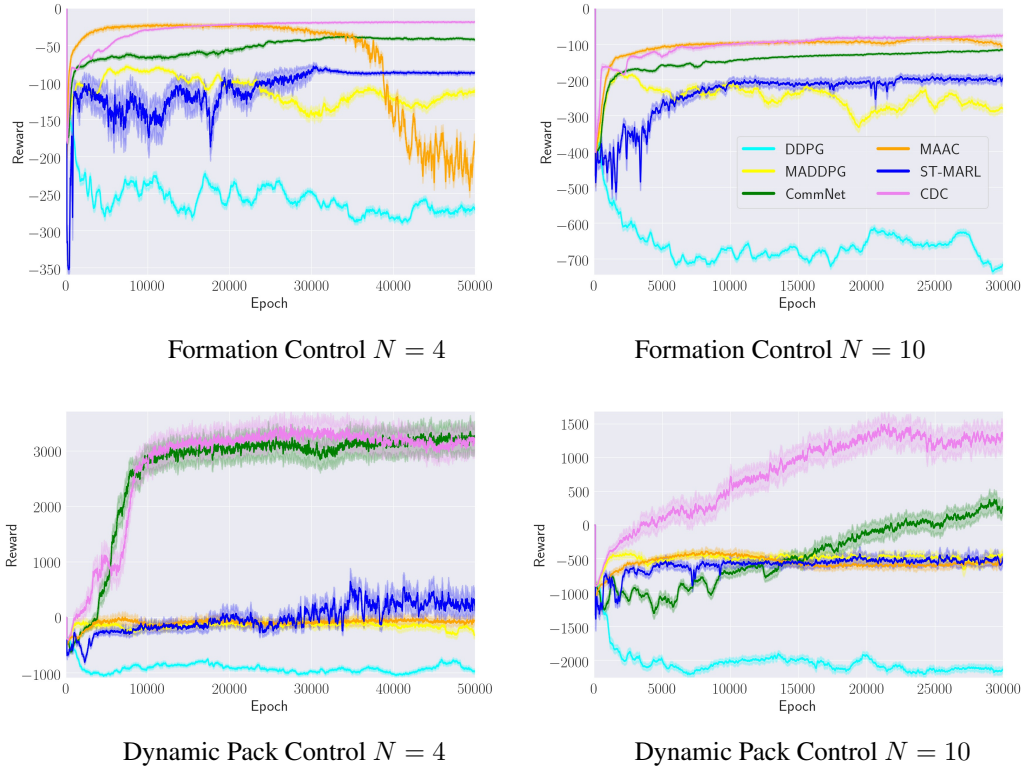


Figure 6: Learning curves on Formation Control and Dynamic Pack Control. The horizontal axes report the number of episodes and vertical axes the achieved rewards. Results are averaged over five different runs.

C.2 Communication networks

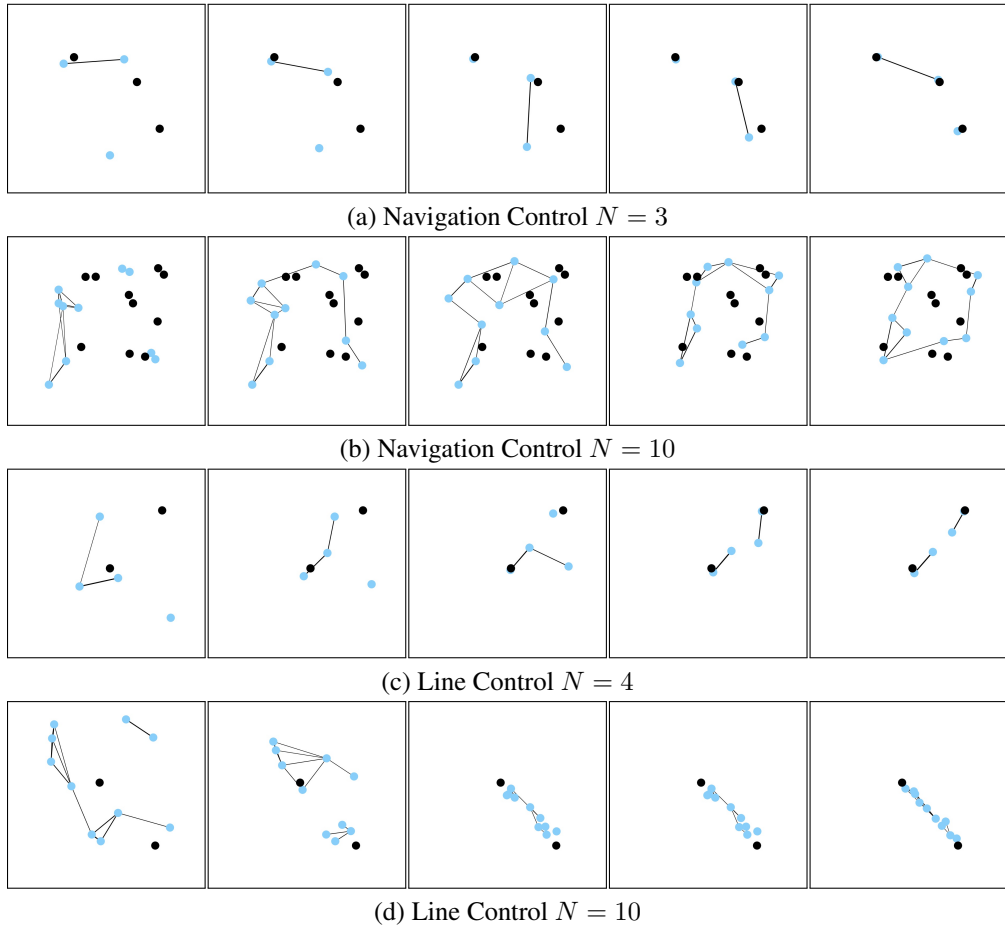
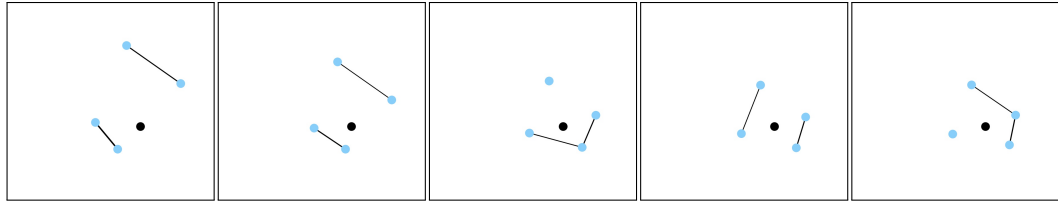
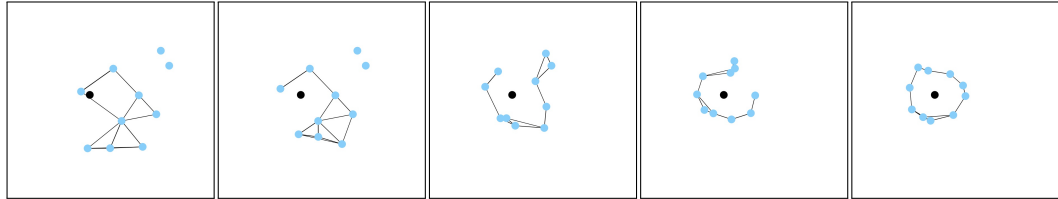


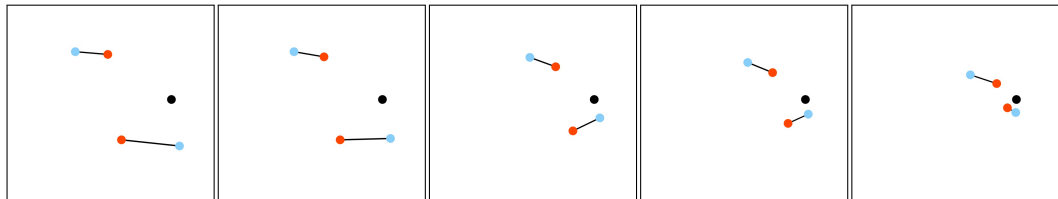
Figure 7: Illustrations of communication networks G_H^t evolving over different episode time-steps.



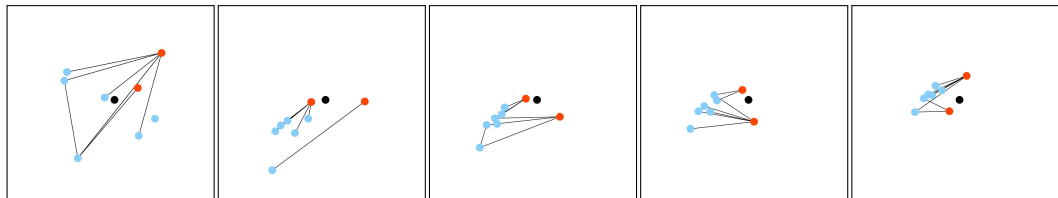
(e) Formation Control $N = 4$



(e) Formation Control $N = 10$



(f) Dynamical Pack Control $N = 4$



(f) Dynamical Pack Control $N = 4$

Figure 8: Illustrations of communication networks G_H^t evolving over different episode time-steps.

C.3 Average communication graphs

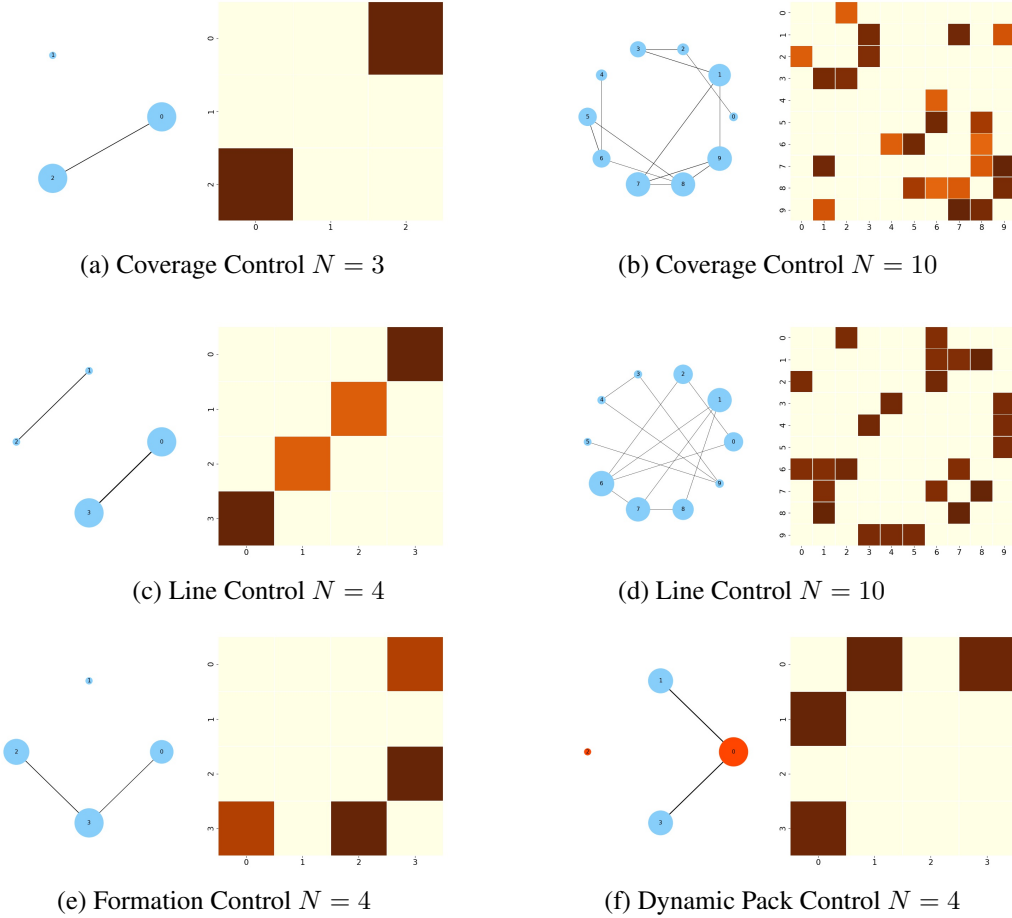


Figure 9: Communication graphs averaged over an episode. For each environment, on the left, node sizes indicate the eigenvector centrality, connections the stable heat kernel values, while numbers the node labels. Here, a circular layout is used to represent the graphs in order to provide an alternative view where connection patterns can result easier to detect. On the right, diffused values are shown as heatmaps, where axis numbers correspond to node labels.

D Ablation study

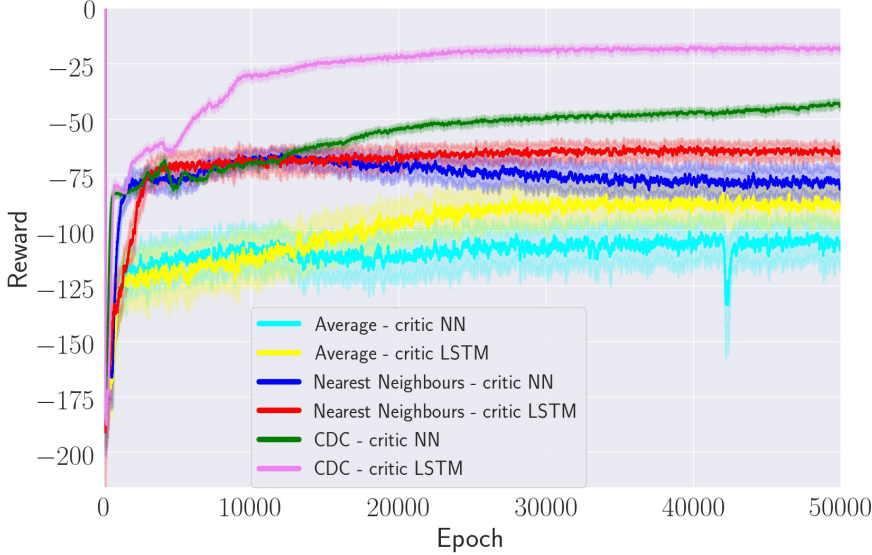


Figure 10: Learning curves of different versions of the proposed model on Formation Control ($N = 4$).

In this section we present the results of an ablation study that has been carried out to investigate the specific benefits of the heat kernel over alternative and simpler information propagation mechanisms. In the *average* version, every agent takes an action after receiving an average of the observations of all other agents, whereas in the *nearest neighbours* version only the observations of an agent’s two nearest neighbours are averaged. For each one of these two mechanisms, we compare a version using the adopted critic (Section 2.4), which uses an RNN (specifically an LSTM), and the version using the traditional critic, which is based on a feed-forward neural network (NN). We also included results to investigate the effects of the LSTM critics on MADDPG.

In Figure 10, it can be noted that the heat kernel achieves the highest performance. Both versions of CDC, with LSTM and without, outperform the others. The results also show that the nearest neighbours version reaches better outcomes compared to the average version; this suggests that averaging all observations lead to nosier embeddings, and limits the effectiveness of the method. Overall, we have observed that using the LSTM-based critic leads to better performance overall. This result is somewhat expected given that the LSTM is able to filter out irrelevant information from a sequence of observations, and can retain only relevant information in its hidden state. From the obtained results, no significant differences have been observed upon changing the order of the agents in all the critic LSTM utilised.

E Choosing the heat kernel threshold

Method	Formation Control $N = 4$		
	Reward	Time	Success Rate
CDC $s = 0.01$	$-4.48 \pm (1.62)$	$13.52 \pm (9.83)$	$0.93 \pm (0.21)$
CDC $s = 0.025$	$-4.33 \pm (1.28)$	$14.01 \pm (9.74)$	$0.94 \pm (0.24)$
CDC $s = 0.05$	$-4.22 \pm (1.46)$	$11.82 \pm (5.49)$	$0.99 \pm (0.1)$
CDC $s = 0.075$	$-4.34 \pm (1.43)$	$12.88 \pm (9.13)$	$0.95 \pm (0.22)$
CDC $s = 0.1$	$-4.31 \pm (1.57)$	$12.52 \pm (8.39)$	$0.96 \pm (0.2)$

Table 2: Comparison of CDC results using different values for threshold s

Table 2 reports on the performance of CDC on Formation Control when the threshold parameter s varies over a grid of possible values (see Eq. 6). In turn, this threshold determines whether the heat kernel values are stable or not. The best performance is obtained using $s = 0.05$, which is the value used in all our experiments. To select the thresholds to test in Table 2, we defined a range of values close to solutions which have been proven to be successful in other heat kernel related works [7, 54].

F Varying the number of agents

# agents	DDPG	CDC
3	2.34 ± 0.61	1.06 ± 0.12
4	3.52 ± 1.67	1.09 ± 0.1
5	3.90 ± 1.68	1.08 ± 0.15
6	4.44 ± 1.7	1.08 ± 0.18
7	5.21 ± 1.98	1.12 ± 0.12
8	6.49 ± 2.17	1.13 ± 0.11

Table 3: Comparison of DDPG and CDC on Dynamic Pack Control. Both algorithms were trained with 4 agents and tested with 3-8. The performance metric used here is the distance of the the farthest agent to the landmark.

We tested whether CDC is capable of handling a different number of agents at test time. Table 3 shows how the performance of DDPG and CDC compares when they are both trained using 4 learners, but 3-8 agents are used at test time. We report on the maximum distance between the farthest agent and the landmark, which is invariant to the number of agents. It can be noted that CDC can handle systems with a varying number of agents, outperforming DDPG and keeping the final performance competitive with other methods that have been trained with a larger number of agents (see Table 1).

G Environment details

Navigation Control. There are N agents and N fixed landmarks. The agents must move closer to all landmarks whilst avoiding collisions. Landmarks are not assigned to particular agents, and the agents are rewarded for minimizing the distances between their positions and the landmarks' positions. Each agent can observe the position of all the landmarks and other agents.

Formation Control. There are N agents and only one landmark. In this scenario, the agents must navigate in order to form a polygonal geometric shape, whose shape is defined by the N agents, and centred around the landmark. The agents' objective is to minimize the distances between their locations and the positions required to form the expected shape. Each agent can observe the landmark only.

Line Control. There are N agents and two landmarks. The agents must navigate in order to position themselves along the straight line connecting the two landmarks. Similarly to Formation Control, the agents objective is to minimize the distances between their locations and the positions required to form the expected shape. Each agent can observe the landmarks only.

Dynamic Pack Control. There are N agents, of which two are leaders and $N - 2$ are members, and one landmark. The objective of this task is to simulate a pack behaviour, where agents have to navigate to reach the landmark. Once a landmark is occupied, it moves to a different location. The landmark location is accessible only to the leaders, while the members are blind, i.e. they can only see their current location.

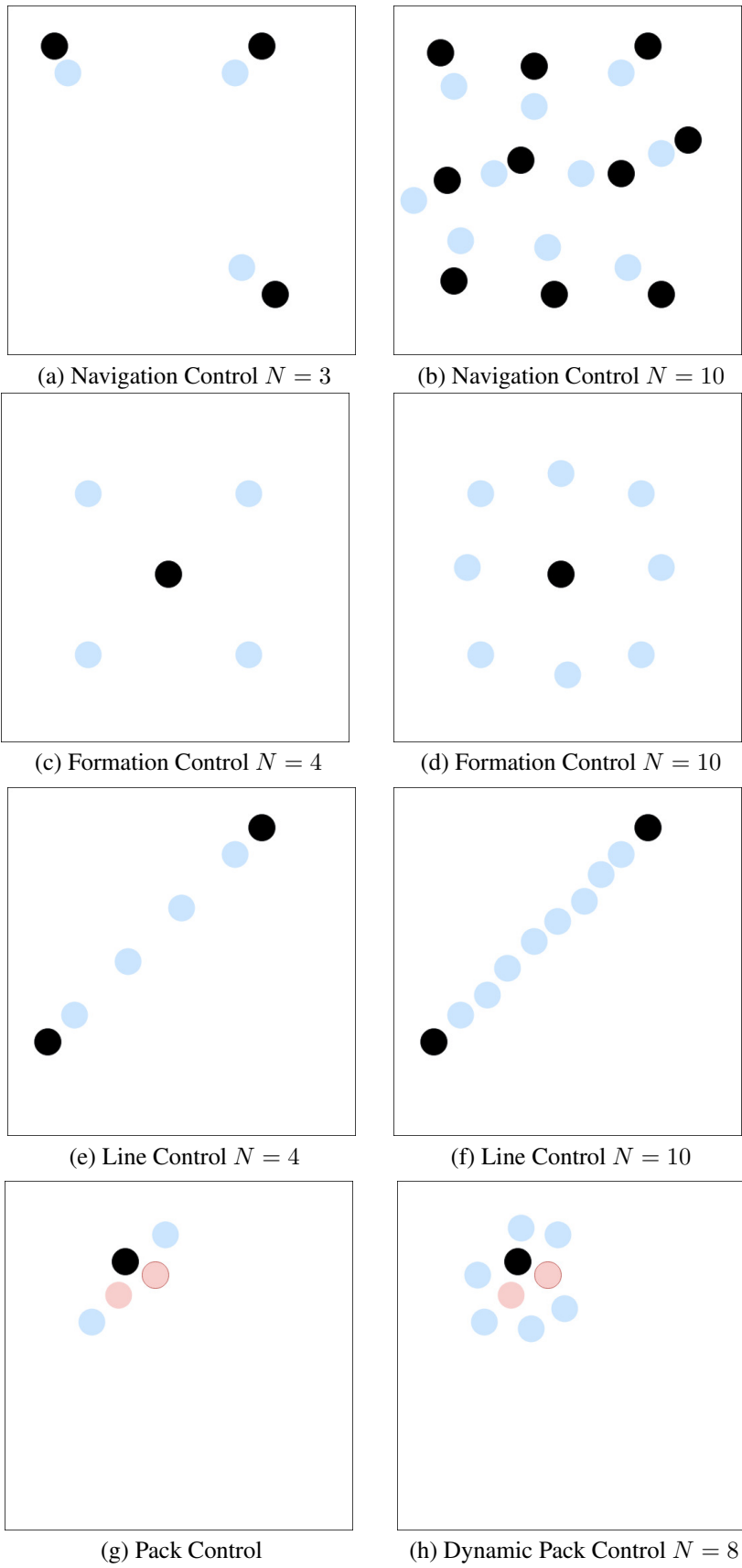


Figure 11: Representations of all the utilised environments.